Research Article Adv. Mater. Lett. 2015, **6**(10), 902-906 Advanced Materials *Letters*

www.amlett.com, www.vbripress.com/aml, DOI: 10.5185/amlett.2015.5833 Published online by the VBRI Press in 2015

Effect of nickel ferrite on bismuth ferrite to generate nanocomposite in relation to structure, characterization, magnetic properties and band gap evaluation

Soumya Mukherjee*, Manoj Kumar Mitra

Department of Metallurgical and Materials Engineering, Jadavpur University, 188, Raja S. C. Mallick Road, Kolkata, 700032, India

*Corresponding author. Tel: (+91) 9830179414; E-mail: smmukherjee3@gmail.com

Received: 02 February 2015, Revised: 12 July 2015 and Accepted: 15 July 2015

ABSTRACT

Multiferroic materials are new class of multi-functional materials which possess both ferro-electric and magnetic properties. This type of material has wide range of applications like semi-conducting to sensors applications. Nanocomposite of equimolar perovskite-spinel is synthesized by chemical route by blending of Nickel ferrite as second phase on Bismuth ferrite after heat treatment at 500 °C for 2, 3 and 4 hours soaking period. From the diffractogram data of XRD, the phase, and planes of orientation are analyzed of the synthesized materials. The crystallite size is calculated by Scherrer's formula. FESEM studies reveal the morphological features having interconnected agglomerates with spherical, irregular polygonal or some elongated shape of the synthesized nanocomposite. FTIR result shows the molecular signature of the nanocrystalline material to verify the M-O coordination. Interplanar spacings and SAED pattern are revealed from HRTEM images which are very close to the experimental findings from XRD phase analysis. UV-VIS analysis is performed in the transmission mode of spectra within the scan range of 200-1100 nm. From the spectra, using Tauc relation band gap is calculated. Band gap are found of the order of 2.847 eV, 2.78 eV, 2.69 eV respectively for 2, 3 and 4 hours soaking period close to semiconducting material. With the increase of soaking time band gap is found to decrease following Arrhenius activation of electronic mobility overwhelming the energy barrier at respective lattice sites. M-H analysis of Nanocomposite at 500 °C for 2 hrs is closer towards ferromagnetic with incomplete loop but for sample at 500 °C for 4hrs it is closer towards superparamagnetic one. The property of this material reflects it has many interesting characteristics suitable for opto-electronic, photo-magnetic devices and other electronic applications.

Keywords: M-H analysis; nanocomposite; perovskite-spinel; band gap; superparamagnetism.

Introduction

Ferrite based Ceramic nanocomposites are gaining vital importance in modern engineering and scientific applications particularly in the field of electronic materials. Perovskite and Spinel based ferrites are found applicable in various domains because of its multiferroic nature like memory devices, catalyst, optical-memory switching, photo-induced devices, multistate memory system etc **[1]**. Till now, researchers have focused more on transitional metal doped perovskite Bismuth Ferrite **[2-4]** at Fe site and rare-earth metal at Bi site **[4]**. These materials are synthesized by solid-state reaction **[5, 6]** sol-gel technique **[7, 8]** hydrothermal technique **[3, 9]** solution combustion **[7]** etc. Substantial amount of research is reported on the evaluation of optical property and band gap for perovskite and spinel based simple ferrites. Optical properties and band gap is evaluated for nanocrystalline Nickel Ferrite powder and film using Tauc relation. Band gap is quite high around 5 eV and 5.7 eV. Band gap is found to vary with thickness of film to a certain extent **[10, 11]**. Similarly, band energy transition for both bulk and nanocrystalline perovskite Bismuth Ferrite is evaluated and reported **[12, 13]**. PL studies of Mn doped Bismuth Ferrite reveals blue emission around 454 nm and weak green emission around 518nm due to self-activation. Light emissions are mainly attributed to Mn^{+2} centre, mainly ascribed to transition of $3d^5$ orbital electrons **[14]**. The use of sol-gel technique can lower the threshold reaction temperature by 200 °C **[15]**. The effect of variation on the percentage of nickel ferrite polyaniline nanocomposites can change the morphology with crystallite size and saturation magnetization behavior **[16]**. The effect of Ni substitution on BFO has shown an increase in the dielectric constant value **[17]**. At different frequency range it is observed that the dielectric constant and tan ð loss are varying monotonically with temperature **[18]**.

Till now, very scanty informations are published on synthesis and evaluation of band gap for the Perovskite-Spinel ferrite nanocomposites. In the present experimental investigations an attempt has been made to synthesize nanocomposite of Bismuth Ferrite-Nickel Ferrite using chemical route. The band gap, M-H analysis of the material is evaluated for optical, magnetic characterizations.

Experimental

Synthesis

Nanocomposite of Bismuth Ferrite-Nickel Ferrite (perovskite-spinel) is synthesized using chemical route. Precursors required for synthesizing the nanocomposite materials are AR grade Bismuth Nitrate Pentahydrate, Ferric Nitrate Nonahydrate, Citric Acid, Ethylene Glycol (All from Merck India) to obtain perovskite part of the nanocomposite while for spinel part- Nickel Nitrate Hexahydrate, Ammonium Hydroxide along with Iron salt (Merck India) are used. At first, equimolar ratio of 1:1 Bi salt and Ferric salts are mixed followed by the addition of 2 moles of citric acid and optimized quantity of ethylene glycol. Citric acid addition leads to conversion of nitrates to citrate salts while glycol will act as chelating complex to entrap the metal ions. After mixing, solution is first heated at about 330 ˚C in a pot furnace for initiation of combustion reaction. Due to this reaction disruption of chelating agent occurs releasing the entrapped citrate metal and finally transformation to respective metal oxides (A). An Ammonium hydroxide solution addition to mixed solution of Nickel Nitrate, Ferric Nitrate in 1:2 molar ratios to generate the precipitation of respective hydroxides. Hydroxide precipitate collected over whatman 40 filter paper is dried at about 80 ˚C to obtain the powder form (B). Both powders (A) & (B) are then mixed properly and subjected to thermal analysis. Annealing of the properly mixed powders is performed in tubular furnace at 500 ˚C for 2, 3 and 4 hours respectively to obtain the crystalline phases for development of the nanocomposite material.

Characterization tools

Samples prepared are characterized by X-Ray Diffractogram (Rigaku, Ultima III, 40KV, 30mA having Cu Kα wavelength 1.54Å,) to identify the phases obtained, plane of orientation of major phases and to determine the crystallite size using Scherrer's equation. Microstructural features of the nanocomposite are revealed by Field Emission Scanning Electron Micrsoscope (FESEM) (Hitachi S-4800, operating voltage 50KV). Nanocomposite sample is placed on the carbon tape and gold coating is done to get clear contrast of the images generated after back scattering. A HRTEM image (Jeol, JEM 2100 and operating voltage 200 KV) is analysed to confirm the structural features and interplanar fringes. The SAED pattern obtained indicates the crystallinity of the phases formed. For FTIR analysis (IR Prestige-21, Shimadzu) the sample is mixed with 0.01 g of KBr (Merck India) to obtain the correct spectra. Pellets are formed after pressing in hydraulic press at about 1.5 tonne/cm^2 for studying the stretching and vibration bonding of the synthesized nanocomposite. UV-VIS study (Lambda 35, UV/VIS Spectrometer, Perkin Elmer) used in transmission mode in the scan range of 200-700 nm to obtain optical spectrograph. Bandgap of the synthesized nanocomposite is calculated using Tauc relation from the spectrograph. M-H analysis is carried by VSM having electromagnet of 2.3 Tesla. (Model No. 7407, Lakeshore).

Results and discussion

Phase evolution & morphological analysis

The thermal heat treatment by DSC-TGA thermal analysis of blended constituents is responsible to generate proper crystallized phase and reported in our earlier publication **[19]**. The heat treated samples are analyzed by XRD. **Fig. 1** gives the XRD result of the synthesized perovskite-spinel type Bismuth Ferrite-Nickel Ferrite nanocomposite by chemical route after annealing at 500 ˚C for 2, 3 & 4 hours soaking periods. Prominent high intensity peaks of perovskite structure Bismuth Ferrite is obtained in comparison to spinel structure Nickel Ferrite for all soaking periods at a fixed annealing temperature as per JCPDS PDF Card No # 01-072-2035 for perovskite Bismuth Ferrite and PDF card No # 01-086-2267 for spinel Nickel Ferrite. Series of crystalline peaks are observed for both ferrites.

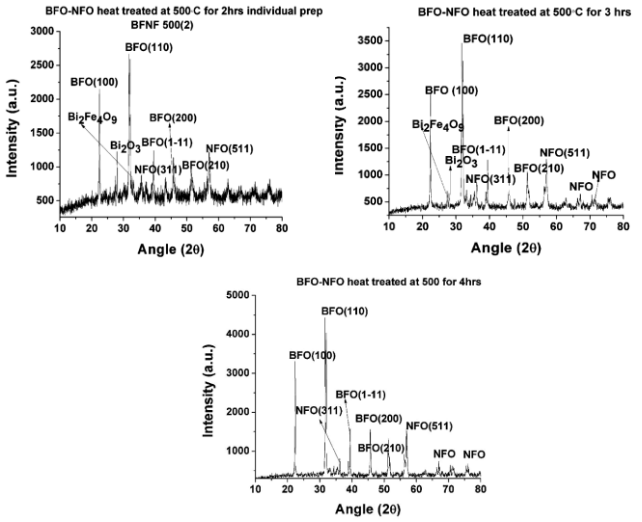

Fig. 1. XRD spectra of the synthesized nanocomposite BFO-NFO after annealing at 500 ˚C for 2, 3 & 4 hours soaking period by chemical route.

From XRD, crystallite size for prominent phases are determined using Scherrer's formula $t = 0.9\lambda/\beta\cos\theta$. Where, 't' is crystallite size, β is the full-width half mean and λ is the Cu Kα source wavelength 1.54 Å. Crystallite size measured for perovskite phase Bismuth Ferrite are about 58.6 and 44 nm and for spinel phase Nickel Ferrite are of 71.6 nm and 59.3 nm. Thus, from XRD analysis it can be inferred that formation of composite occurs having nanodimension crystallite sizes for both phases. Perovskite phase have grown along (110), (100), (1-11), (200), (210) planes with minimum energy while for spinel phase planes of orientation are along (311) & (511) respectively. No intermediate phases are found to be observed even in thorough XRD analysis which may be responsible for causing degradation of property. Morphology of the synthesized nanocomposite is studied using Field Emission Scanning Electron Microscope as shown in **Fig. 2**.

Interconnected agglomerations have been observed for all samples synthesized by chemical route at given temperature with variable annealing time. Particulates are of 50nm in size having spherical, irregular polygonal or some elongated shapes are observed after 2 hours soaking. Agglomerates have dense with few interconnected pores are found to have tripod type shape for all cases. Particulates have size dimensions of 60 nm, 75 nm after 3 hours and 4 hours soaking with similar morphology for all conditions. Spherical morphology is found for perovskite Bismuth Ferrite and irregular polygon shapes for spinel component of the nanocomposite **[20, 21]**. Thus two distinct morphologies for the both ferrites indicate formation of nanocomposite material.

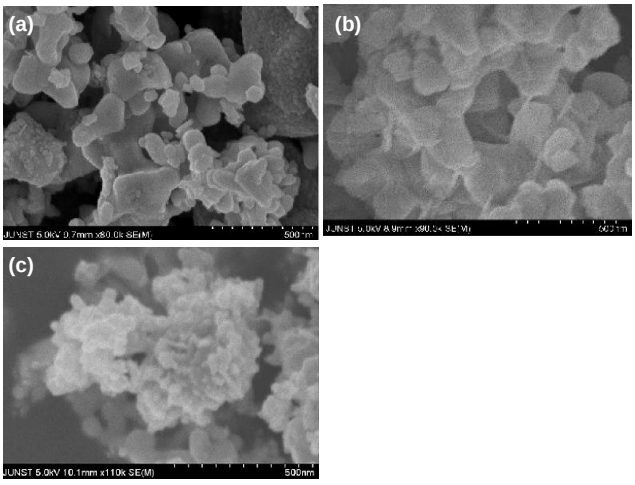

Fig. 2. FESEM morphology of BFO-NFO nanocomposite annealed at 500 °C for 4 hrs (a), for 3 hrs (b) and for 2 hrs soaking period (c).

FTIR studies

The result of FTIR spectra of the nanocomposites are shown in **Fig. 3**. Spectral analysis is performed in the scan range of 4500-400 cm^{-1} after preparing with KBr pellet. Main absorption spectra are observed within 1000 cm^{-1} at about 450 cm^{-1} and 550 cm^{-1}. Previous researchers had observed that stretching vibrations for M-O having tetrahedral co-ordination and for M-O octahedral co-ordination were in the scan range of 620-550 cm^{-1} and 450-385 cm^{-1} **[22-24]**. Hence, the observed stretching behavior at 450 cm^{-1} and 550 cm^{-1} identified corresponds to vibration stretching of M-O octahedral and M-O tetrahedral co-ordination sites. Hence, FTIR analyses are found to be in confirmation with the proper phase identification of the composite material inferred earlier from XRD studies.

Evaluation of band gap & microstructure studies HRTEM

UV-VIS spectral analysis are scanned for the synthesized sample in the range of 200-1100 nm in transmittance mode. Samples are made to treat in ultrasonicator bath (45 minutes) in de-ionized water medium for preparing the test sample to obtain optical property measurement. Band gap is evaluated from the spectra using Tauc relation $(\alpha h\nu) = B(E_g - h\nu)^n$ where n=2 for allowed indirect transition, n=1/2 for allowed direct transition while n=3 & 3/2 for forbidden indirect, direct transition probability. $(\alpha h\nu)^2$ versus Eg plot (**Fig. 4**) exhibits a good fit with the direct band gap evaluation process.

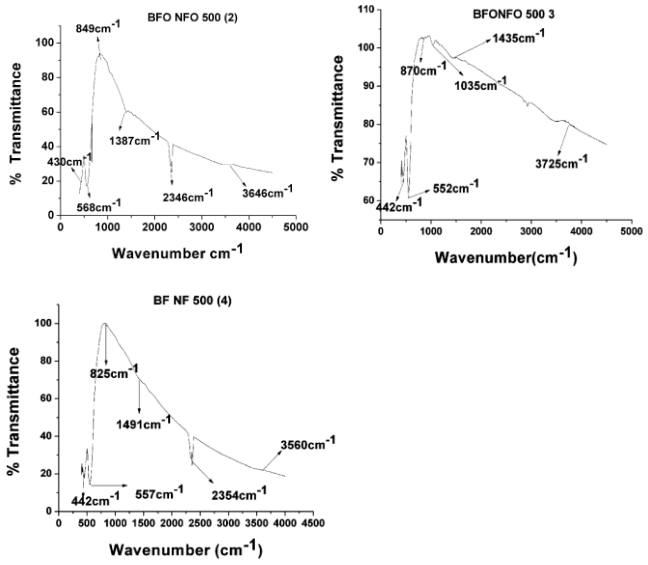

Fig. 3. FTIR spectra of the synthesized Bismuth Ferrite-Nickel Ferrite nanocomposite at 500 ˚C for 2, 3 and 4 hours soaking period.

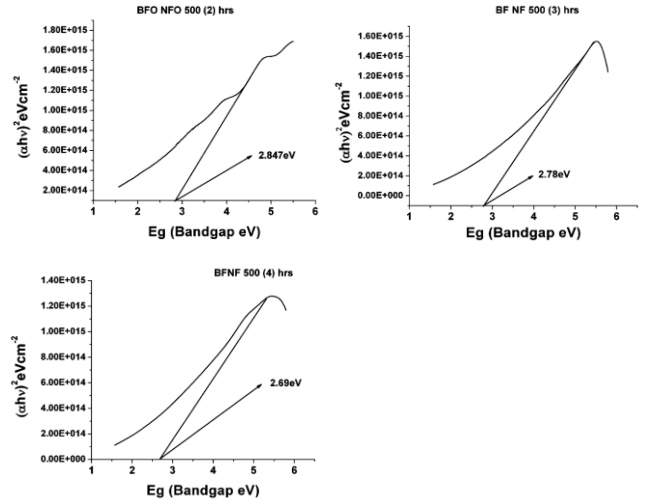

Fig. 4. Band gap of the synthesized nanocomposite annealed at 500 ˚C with different soaking period of 2 hrs, 3 hrs and 4 hrs, respectively.

Extrapolation of the linear region of the plot to the zero absorption point in X-axis (E_g) i.e. will provide the calculated band gap. Band gap evaluated for the nanocomposite with variable period for annealing are 2.847 eV, 2.78 eV and 2.69 eV respectively. Calculated band gap is close to semiconducting material band gap range 1-3 eV. Previously researchers have evaluated the band gap of perovskite phase Bismuth Ferrite and spinel phase Nickel Ferrite synthesized by various physical and chemical processes. Band gap evaluated for thin film of Nickel Ferrite is 5.7 eV and it does not vary with thickness **[10]**. As semiconductor material band gap Eg for Nickel Ferrite is 2.1 eV **[25, 26]**. Band gap of perovskite Bismuth Ferrite is reported to be about 2.8 eV **[12]**. For nanocrystalline Bismuth Ferrite Eg is reported to be about 3.10 eV **[13]**. Thus, the evaluated band gap is found to be in correspondence with the above experimental findings. The

material has the possibility for application as catalyst in near visible zone and also for degradation of organic pollutants as well as treatment of ferruginous sludges in mining industries.

HRTEM image analysis (**Fig. 5**) shows similar morphology observed from FESEM studies. Powdered samples are sonicated for 45 minutes and added dropwise on copper coated carbon template for the characterization. Interplanar fringes obtained at higher resolution found to be in line with the experimental observations from XRD spectra. SAED pattern shows crystalline nature of the phases and planes of orientation for the nanocomposite.

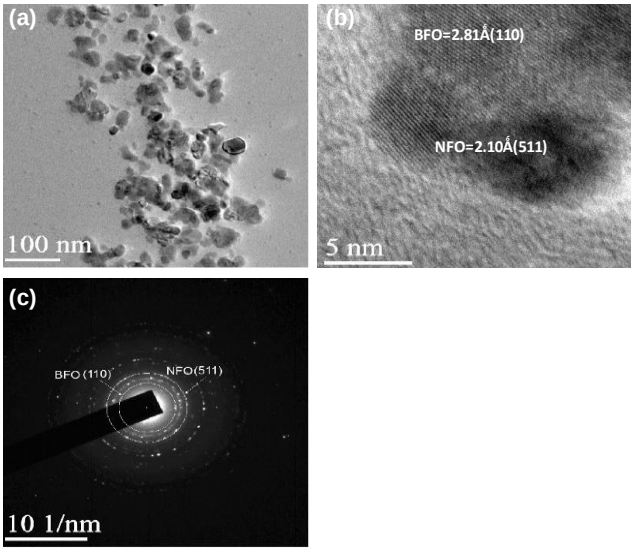

Fig. 5. HRTEM (a) morphology, (b) interplanar fringes and (c) SAED pattern of BFO-NFO Nanocomposite at 500 ºC for 2 hrs.

Magnetic property and measurements

M-H curve is obtained for analyzing the magnetic behavior of the nanocomposite prepared at its highest level of purity. For the present sample of Bismuth Ferrite-Nickel Ferrite prepared at 500 ˚C for 2 hours (**Fig. 6**), saturation value of magnetization could not be obtained at room temperature while the loop is also not completely ferromagnetic in nature. Coercive field H_C for Nanocomposite of Bismuth ferrite-Nickel Ferrite is about 369 KOe while remanant magnetization M_R is 0.112 emu/g. From M-H curve for the sample of Bismuth Ferrite-Nickel Ferrite synthesized at 500 ˚C for 4 hours, saturation value of magnetization is observed. Magnetic saturation obtained is M_S 1.27 emu/g while coercive field H_C obtained is 959.57 Oe. Remnant magnetization value obtained for this sample is 0.6327 emu/g. Thus, the squareness ratio obtained is M_S/M_R = 0.4981. This sample exhibits magnetic property close to super paramagnetism in compare to sample synthesized at 500 ˚C for 2 hrs which is closer towards ferromagnetic nature. This finding of the M-H curve behavior at higher soaking period is close to experimental findings of Amit Kumar *et al.* **[27]**. M-H curve obtained at 500 ˚C for 4 hours (**Fig. 7**) is found to be in line with the findings of Hemant Singh *et al*. They observed that magnetic saturation increases while coercivity decreases with increase in Nickel ferrite content in the system. The increase in magnetization is mainly responsible due to spontaneous magnetization of the nanocomposite originating from the antiparallel spin of unbalanced spin of the ferromagnetic Ni-ferrite. This reason is also found to be valid for the present M-H curve behaviour for BFO-NFO at two different soaking periods. In other words interaction of the magnetic poles becomes energetic in the powder **[28]**. This plot exhibits soft magnetic nature while magnetic characteristics indicate strong ordered magnetic structure in the nanocomposite.

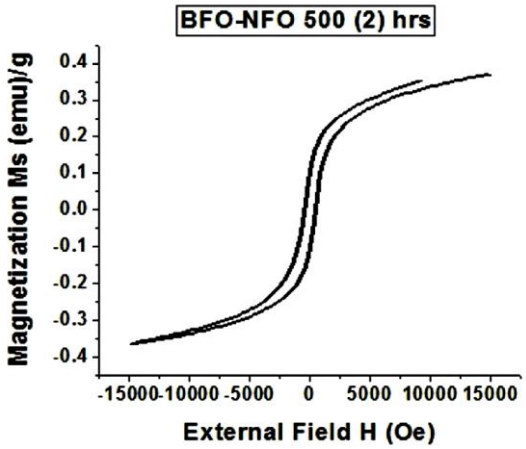

Fig. 6. M-H curve of nanocomposite of BFO-NFO at 500°C for 2 hours.

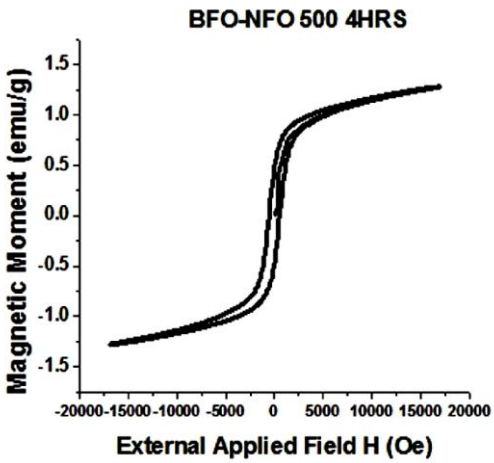

Fig. 7. M-H curve of nanocomposite of BFO-NFO at 500 °C for 4 hours.

Conclusion

Nanocomposite of Bismuth Ferrite-Nickel Ferrite is synthesized by chemical route at 500 ºC for different soaking period successfully. XRD study identified the phases formed and crystallite size measured are about 58.6 nm, 44 nm for BFO and 71.6 nm, 59.3 nm for NFO. Interconnected agglomerations have been observed for all samples. Particle sizes of about 50, 60 and 75 nm for 2, 3, and 4 hrs soaking periods respectively. FTIR analysis exhibits the stretching and vibration of M-O octahedral, M-O tetrahedral coordination sites. Band gap evaluated using Tauc relation are 2.847 ev, 2.78 eV and 2.69 eV respectively and HRTEM studies confirm interplanar fringes to d-planar spacing and SAED pattern shows planes of orientation and crystallinity of the phases for the nanocomposite. M-H analysis confirms superamagnetic behavior of the samples synthesized at 500 ˚C for 4 hrs.

The aforesaid synthesized material with considerations to the above mentioned properties is found to be a promising candidate for ferrous-sludge removal, photo-induced catalyst for organic and ferro-oranic complexes wastes besides being a promising candidate for photo-induced magnetic devices.

Acknowledgements

Author is thankful to the Department of Metallurgical & Material Engineering for providing the infrastructure for the research facilities and to the State Government Fellowship of West Bengal for financial support. They are also thankful to UGC-UPE and DST Nanomission for infrastructure support. Author is also greatful to Dr. Dipten Bhattacharya, Principal Scientist, Nano-Structured Materials division, Central Glass & Ceramic Research Institute, Kolkata to facilitate M-H analysis.

Reference

1. Pullar, C. Robert.; *Prog. Mater Sci.*, **2012**, *57*, 1191. **DOI:** 10.1016/j.pmatsci.2012.04.001
2. Cheng, Bing Luo.; Le, Chang Chen.; Zhi, Xu.; Qian, Xie.; *Phys. Lett. A.*, **2010**, *374*, 4265. **DOI:** 10.1016/j.physleta.2010.08.045
3. Yan, Xiaolong.; Chen, Jianguo.; Qi, Yufa.; Cheng, Jinrong.; Meng, Zhongyan.; *J. Eur. Ceram. Soc.* **2010**, *30*, 265. **DOI:** 10.1016/j.jeurceramsoc.2009.06.016
4. Kumar, Amit.; Yadav, K.L.; *Mat. Sci. Eng B*, **2011**, *176*, 227. **DOI:** 10.1016/j.mseb.2010.11.012
5. Li, J.; Duan, Y.; He, H.; Song, D.; *J. Alloy. Compd.*, **2001**, *315*, 259. **DOI:** 10.1016/S0925-8388(00)01313-X
6. Valant, Matjaz.; Axelsson, Karin Anna.; Alford, Neil.; *Chem. Mater.*, **2007**, *19*, 5431. **DOI:** 10.1021/cm071730+
7. Sen, K.; Singh, K.; Gautam, Ashish.; Singh, M.; *Ceram. Int.*, **2012**, *38*, 243. **DOI:** 10.1016/j.ceramint.2011.06.059
8. Kumar, Manoj.; Yadav, L. K.; *J. Phys. Chem. Solids.*, **2007**, *68*, 1791. **DOI:** 10.1016/j.jpcs.2007.05.006
9. Du, Yi.; Cheng, Yiang Zhen.; Shahbazi, Mahboobeh.; Collings, W Edward.; Miotello, A.; Dou, Xue Shi.; Wang, Lin. Xiao.; *J. Alloy. Compd.*, **2010**, *490*, 637. **DOI:** 10.1016/j.jallcom.2009.10.124
10. Dixit, Gagan.; Singh, P. J.; Srivastava, C. R; Agarwal, M. H.; Chaudhary, J. R.; *Adv. Mat. Lett*, **2012**, *3*, 21. **DOI:** 10.5185/amlett.2011.6280
11. Srivastava, Manish.; Ojha, K. Animesh.; Chaubey, S.; Materny, A.; *Vacuum*, **200**9, *481*, 515. **DOI:** 10.1016/j.jallcom.2009.03.027
12. Catalan, G.; Scott, F. J.; *Adv. Mater.* **2009**, *21*, *529*, 2463. **DOI:** 10.1002/adma.200802849
13. Mukherjee, A.; Hossain, M. S.; Pal M.; Basu, S.; *Appl. NanoSci.*, **2012**, 2, 305. **DOI:** 10.1007/s13204-012-0114-8
14. Xuelian, Yu.; Xiaoqiang, An.; *Solid. State. Commun.*, **2009**, *149*, 711. **DOI:** 10.1016/j.ssc.2009.02.010
15. Suresh Pittala; Srinath S; *Adv.Mat.Lett.* , **2014**, *5*, 127. **DOI:**10.5185/amlett.2013.fdm.34
16. Kondwar B Subhash; Nandapure I Arti; Nandapure I Bharti; *Adv.Mat. Lett*; **2014**, *5*, 339. **DOI:** 10.5185/amlett.2014.1035
17. Biswal R M; Nanda J; Mishra C N; Anwar S ; Mishra A; *Adv.Mat.Lett.*, **2014**, *5*, 531. **DOI:** 10.5185/amlett.2014.4566
18. Kumari B; Mandal R P; Nath K T; *Adv Mat.Lett.*, **2014**, *5*, 84. **DOI:** 10.5185/amlett.2013.fdm 36
19. Mukherjee, Soumya.; Mitra Kumar Manoj.; *Interceram.*, **2013**, *62*, 376.
20. Mukherjee, S.; Chakraborty, S.; Mukherjee, S.; *International Journal of Current Engineering and Technology.*, **2012**, *2*, 403. **DOI:** 10.14741
21. Mukherjee, Soumya.; Mitra, Kumar Manoj.; *International Journal of Advances in Science and Technology.*, **2013**, *6*, 15. **ISSN:** 2229 5216
22. Jacob, P Banu.; Kumar, Ashok.; Pant, P. R.; Singh, Sukhvir.; Mohammed, M. E.; *B. Mater. Sci.*, **2011**, *34*, 1345. **DOI:** 10.1007/s12034-011-0326-7
23. Zahi, S.; *J. Electromagnetic Analysis & Applications.*, **2010**, *2*, 56. **DOI:** 10.4236/jemaa.2010.21009
24. Lazarevic, Z. Z.; Jovalekic, C.; Milutinovic, A.; Romcevic, J. M.; Romcevic, N. Z.; *Acta. Phys. Pol. A.*, **2012**, *121*, 682. **PACS numbers:** 75.20.-g, 81.07.Wx, 81.20.Ev, 74.25.nd
25. Bharathi, K. Kamala.; Vemuri, S. R.; Ramana, V. C.; *Chem. Phys. Lett.*, **2011**, *504*, 202. **DOI:** 10.1016/j.cplett.2011.02.003
26. Dolia, N. S.; Sharma, Rakesh.; Sharma, P. M.; Saxena, S. N.; *Indian J. Pure. Ap. Phys.*, **2006**, *44*, 774. **IPC Code:** H01F 41/30
27. Kumar, Amit.; Yadav, L. K.; *Physica B.*, **2010**, *405*, 465. **DOI:** 10.1016/j.physb.2010.08.054
28. Singh, Hemant.; Yadav, K.L.; *J. Alloy. Compd,.* **2014**, *585*, 805. **DOI:** 10.1016/j.jallcom.2013.09.201

